ACS APPLIED MATERIALS & INTERFACES

Letter

www.acsami.org

Improving the Solubility of Mn and Suppressing the Oxygen Vacancy Density in $Zn_{0.98}Mn_{0.02}O$ Nanocrystals via Octylamine Treatment

Yan Cheng,[†] Weichang Hao,*[,†,‡] Huaizhe Xu,*[,†] YouXing Yu,[§] Tianmin Wang,[†] Rui Chen,[⊥] Linjuan Zhang,[∥] Y. Du,[‡] X. L. Wang,[‡] and S. X. Dou[‡]

[†]Department of Physics and Center of Materials Physics and Chemistry, Beihang University, Beijing 100191, P. R. China

[‡]Institute for Superconducting and Electronic Materials (ISEM), University of Wollongong, Wollongong, NSW 2522, Australia

[§]School of Materials Science and Engineering, Beihang University, Beijing 100191, P. R. China

[⊥]State Key Laboratory of Inorganic Synthesis and Preparative Chemistry, College of Chemistry, Jilin University, Changchun 130012, P. R. China

[∥]Beijing Synchrotron Radiation Facility, Institute of High Energy Physics, Chinese Academy of Sciences, Beijing 100049, P. R. China

Supporting Information

ABSTRACT: $Zn_{0.98}Mn_{0.02}O$ nanocrystals were synthesized by the wet chemical route and were treated with different content of octylamine. The environment around Mn and the defect type and concentration were characterized by photoluminescence, Raman, X-ray photoelectron spectroscopy, and X-ray absorption fine structure. It is found that N codoping effectively enhances the solubility of Mn substituting Zn via reducing donor binding energy of impurity by the orbital hybridization between the N-acceptor and Mn-donor. On the other hand, the O atoms released from MnO_6 and the N ions from octylamine occupy the site of oxygen vacancies and result in reduction of the concentration of oxygen vacancies in $Zn_{0.98}Mn_{0.02}O$ nanocrystals.

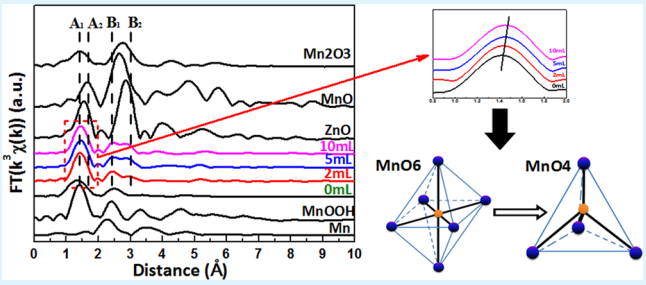

KEYWORDS: *co-doping, oxygen vacancy, solubility, XAFS*

1. INTRODUCTION

As an important wide-band-gap semiconductor material (band gap 3.37 eV), ZnO has many attractive properties, such as near-ultraviolet (UV) emission, transparent conductivity, UV sensitivity, and gas sensitivity.[1,2] Mn-doped ZnO has been investigated extensively due to the potential applications as spintronics materials.[3] However, the solubility of Mn in ZnO is lower in the nanocrystals than that in the bulk because of the self-purification process of Mn ions.[4,5] Zhang[6] has proved that the solubility of Mn in Mn-doped ZnO nanocrystals is less than 1%. In addition, some defects such as oxygen vacancy (V_O) can be easily formed due to the low formation energy[7] during doping. The presence of V_O has great effects on the properties of Mn-doped ZnO.[8,9] It is very important to find an effective method of enhancing the solubility of Mn and suppressing the formation of V_O in Mn-doped ZnO. Codoping can modify the state of the dopants in host lattices and modulate the defect type and concentration. It has been reported recently that the codopant Te in N-doped ZnO could effectively increase the solubility of N and suppress the formation of defects in N-doped ZnO.[10] Chen et al.[11] have indicated (F, Li) codoping can suppress the Li interstitials in ZnO. Sato et al.[12−15] theoretically proposed that codoping Ga in N-doped ZnO could dramatically increase the solubility of N in ZnO by the formation of the acceptor−donor−acceptor (A−D−A) complex, which reduced the ionization energy of the acceptor impurities. In the ZnO system, transition metal Mn doping forms a donor level, while N doping forms an acceptor level. We suppose that a Mn-donor level and N-acceptor level may form the donor−acceptor−donor (D−A−D) complex, which has a similar structure to A−D−A, and thus it could increase the solubility of Mn in ZnO during (Mn, N) codoping by reducing the ionization energy of the donor impurities.

However, it is difficult to measure the solubility and the defect type and concentration. X-ray absorption fine structure (XAFS) is very sensitive to the local environment of a selected atom.[16] The oxidation states and the local coordination of the selected atom can be exactly studied even in a diluted content. For example, Sun[17] has found that the substitutional Co ions in ZnO tended to gather together via investigating the Co occupation sites and distributions in $Zn_{1-x}Co_xO$ thin films by XAFS. Hsu[18] has also proved the existence of oxygen vacancies by Co and Zn k-edge XAFS. In this paper, we have synthesized $Zn_{0.98}Mn_{0.02}O$ by the wet chemical route and have treated them with different contents of octylamine. We have systematically investigated the variations of the environment around Mn and

Received: July 26, 2012
Accepted: September 7, 2012
Published: September 7, 2012

the concentration of V_O in $Zn_{0.98}Mn_{0.02}O$ nanocrystals via Mn and Zn k-edge XAFS, Raman, and photoluminescence spectra. We found that codoping can effectively change the state of Mn dopants in ZnO and tune defect type and concentration.

2. EXPERIMENTAL SECTION

$Zn_{0.98}Mn_{0.02}O$ nanocrystals were synthesized by the wet chemical route as described by Schwartz.[19] The precursor salts (zinc acetate and manganese acetate) were dissolved in dimethylsulfoxide (DMSO) according to the desired stoichiometry. The total metal ion concentration was 0.1 M. Tetramethylammonium hydroxide (TMAH) was dissolved in ethanol, keeping the concentration at 0.55 M. Then the ethanolic solution of TMAH was added dropwise to the metal salt solution under constant stirring at room temperature. After 48 h, the nanocrystals were precipitated by adding ethylacetate and removed from the supernatant by centrifugation. Octylamine in different amounts (0, 2, 5, and 10 mL) was added to the $Zn_{0.98}Mn_{0.02}O$ precipitates in a 1:1 mixture of ethanol and DMSO solutions. The mixture was stirred at 318 K for 2 h, then centrifuged and dried at 353 K. Finally, the precipitates were annealed at 873 K in air for 3 h to remove the precursor.

The X-ray diffraction (XRD) patterns were recorded by a Rigaku Dmax/C X-ray diffractometer using Cu Kα radiation operated at 40 kV and 200 mA. Mn and Zn k-edge XAFS spectra were collected on Beamline 1W1B at the Beijing Synchrotron Radiation Facility. For the Mn k-edge, the XAFS spectra were measured in fluorescence mode due to the lower concentration of Mn, while the spectra of Zn k-edge were collected in transmission mode. The chemical state of N was characterized by X-ray photoelectron spectroscopy (XPS) (MK II XPS with Al (Kα) source). Photoluminescence and Raman spectra were detected by a HR800 LabRam Infinity spectrometer excited by a continuous He−Cd Laser with a wavelength of 325 nm and by a continuous Ar^+ laser with a wavelength of 514 nm, respectively.

3. RESULTS AND DISCUSSION

Figure 1 shows the XRD patterns of $Zn_{0.98}Mn_{0.02}O$ nanocrystals treated with 0, 2, 5, and 10 mL of octylamine, respectively. All the diffraction peaks could be attributed to pure ZnO in the wurtzite structure. The (002) diffraction peak, as shown in the inset, shifts toward a small angle with increasing content of octylamine, indicating an expansion of the lattice. No secondary phase is detectable under the resolution of XRD.

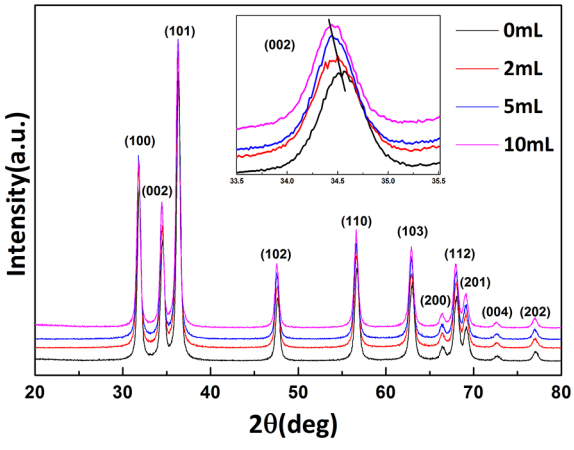

Figure 1. XRD patterns of $Zn_{0.98}Mn_{0.02}O$ nanocrystals treated with different content of octylamine. Inset is a comparison of the (002) peak for the four samples.

Figure 2(a) shows the corresponding PL spectra of $Zn_{0.98}Mn_{0.02}O$ nanocrystals treated with different content of octylamine. Each PL spectrum can be divided into two luminescence bands (UV emission at about 390 nm and visible emissions at about 530 and 580 nm). The UV emission comes from the near-band-edge free excitation transition. The red-shift of UV emission with increasing content of octylamine indicates the decrease of band gap width, and this could be attributed to the strong hybridization between the d electrons of Mn and the p electrons of N dissolved into ZnO, where the hybridization narrows the band gap.[20] The emission at about 530 nm appears in both untreated and octylamine-treated $Zn_{0.98}Mn_{0.02}O$ samples, which is considered from the V_O.[21−23] The emission at about 580 nm only appears in samples treated with octylamine, as shown in Figure 2(b). We attribute this emission to the defects possibly generated from the incorporation of N atoms in $Zn_{0.98}Mn_{0.02}O$ nanocrystals.[24]

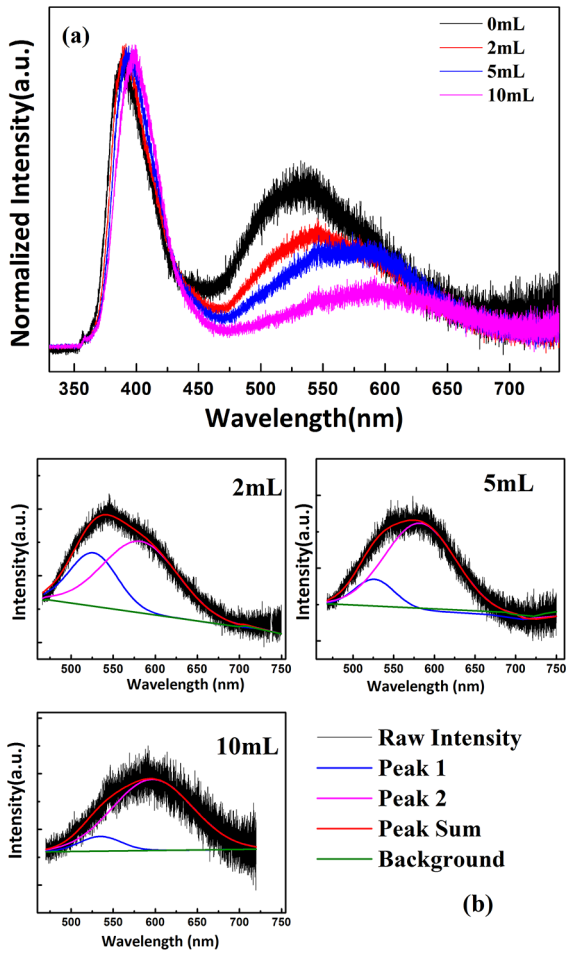

Figure 2. (a) Photoluminescence spectra of $Zn_{0.98}Mn_{0.02}O$ nanocrystals treated with different content of octylamine. (b) The Gauss fitting of PL spectra of peaks at 530 and 580 nm of $Zn_{0.98}Mn_{0.02}O$ nanocrystals treated with different content of octylamine.

To confirm the incorporation of N atoms in $Zn_{0.98}Mn_{0.02}O$ nanocrystals after octylamine treatment, we have measured the N 1s XPS spectrum of $Zn_{0.98}Mn_{0.02}O$ nanocrystals treated with 2 mL of octylamine. As shown in Figure 3, two weak peaks are

dx.doi.org/10.1021/am301471v | ACS Appl. Mater. Interfaces 2012, 4, 4470−4475

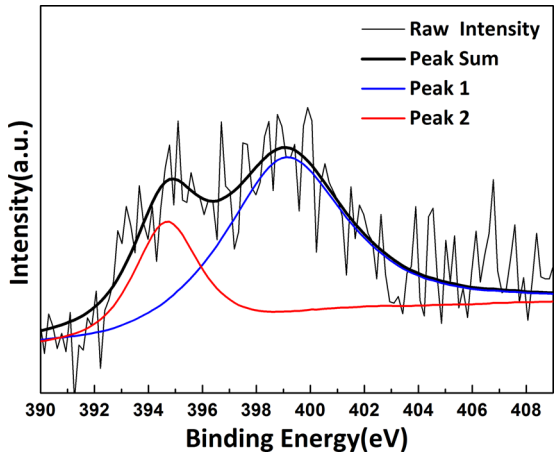

Figure 3. XPS spectra and simulated lines of N 1s for $Zn_{0.98}Mn_{0.02}O$ nanocrystals treated with 2 mL of octylamine.

observed: the peak at 399 eV corresponds to the N-related bonding,[25] and the peak at 394.6 eV represents the Zn−N bonding due to N substituting O sites.[26] Figure 3 shows clearly that some N ions have incorporated into the $Zn_{0.98}Mn_{0.02}O$ nanocrystals after treatment with 2 mL of octylamine.

Figure 4(a), (b), and (c) shows the dependence of $Zn_{0.98}Mn_{0.02}O$ nanocrystal lattice constants *a* and *c* and the

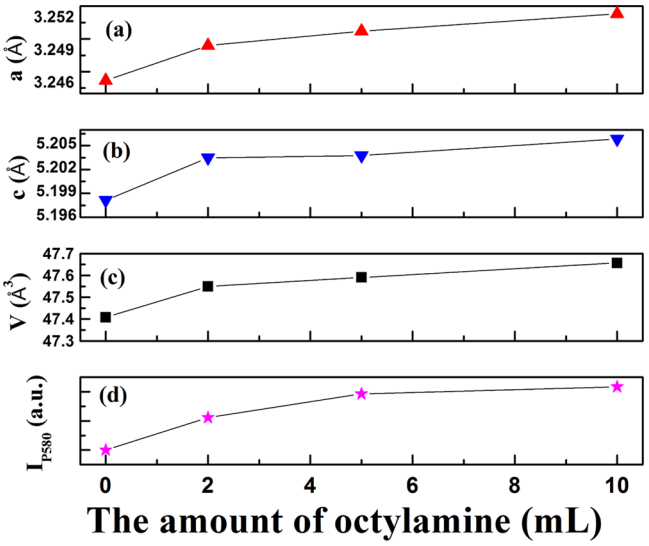

Figure 4. Variations of the lattice constants *a* and *c* and the unit cell volume (*V*) and the intensity of emission at 580 nm in PL spectra (I_{PS80}) of the nanocrystals treated with different content of octylamine.

unit cell volume (*V*) on the octylamine content deduced from XRD patterns. The lattice constants *a* and *c* and the unit cell volume increase with increasing octylamine content. The lattice of $Zn_{0.98}Mn_{0.02}O$ expands when O is substituted by N because the radius of N (0.75 Å) is bigger than that of O (0.73 Å). The increase of lattice constants and cell volume further demonstrates that some N atoms substitute O in the ZnO lattice. Figure 4(d) shows the intensity of the PL peak at 580 nm (I_{PS80}) as a function of the octylamine content. The intensity of PL emission at 580 nm also increases with the octylamine content, indicating the increase of the defects due to N dissolved into the ZnO lattice, which is well consistent with XRD results as shown in Figure 4(a)−(c). All these results reveal that more N atoms dissolved into ZnO with more treatment of octylamine content.

Figure 5 shows the room-temperature Raman spectra of $Zn_{0.98}Mn_{0.02}O$ nanocrystals treated with different content of

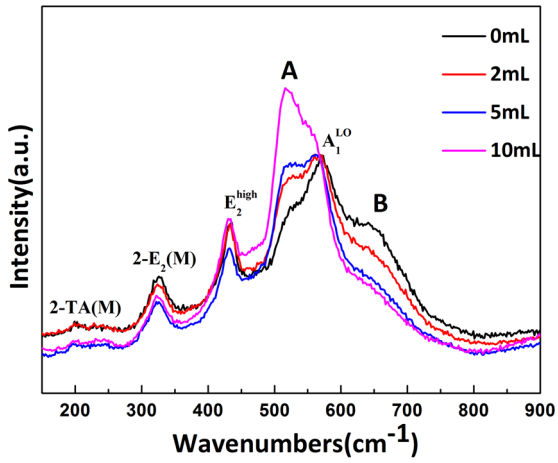

Figure 5. Raman spectra of $Zn_{0.98}Mn_{0.02}O$ nanocrystals treated with different content of octylamine.

octylamine. The two bands at 433 and 566 cm^{-1} correspond to E_2^{high} and A_1^{LO} modes.[27,28] The 201 and 323 cm^{-1} peaks are assigned to the second-order Raman modes arising from the zone-boundary phonons 2-TA(M) and 2-E_2(M).[29,30] The mode at 232 cm^{-1} is assigned to the acoustic-phonon branch at the zone boundary.[31,32] The two additional peaks at 521 and 643 cm^{-1}, labeled as A and B, are assigned to the defects due to Mn^{2+} dissolved into the ZnO lattice[33−35] and the oxygen vacancies,[30,36] respectively. The increase of peak A intensity and the decrease of peak B intensity suggest that the Mn content dissolved into ZnO increases, and the V_O density decreases with increasing octylamine content.

To investigate the variation of the concentration of V_O, we have compared the Zn k-edge X-ray absorption near edge structure (XANES) spectrum of pure ZnO with those of $Zn_{0.98}Mn_{0.02}O$ nanocrystals treated with different content of octylamine. As shown in Figure 6, the XANES spectra of all octylamine-treated samples are similar to the reference spectrum of ZnO, while the intensity of the white line of

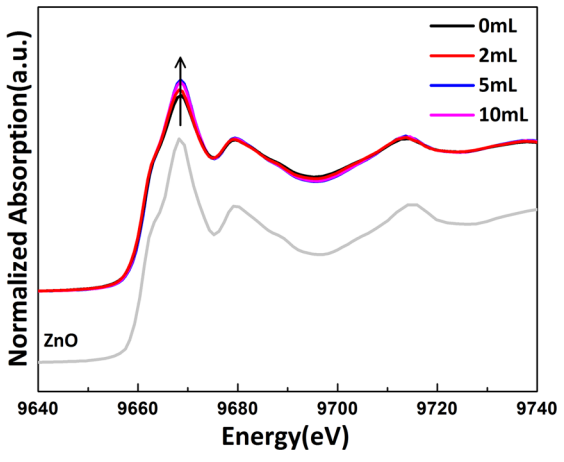

Figure 6. Zn k-edge XANES spectra of $Zn_{0.98}Mn_{0.02}O$ nanocrystals treated with different content of octylamine and reference ZnO.

octylamine-treated samples increases with increasing octylamine content. As the amplitude of the photoelectron scattering from Zn is much smaller than that from O, the intensity of the white line is mainly determined by the number of the O atoms surrounding the Zn atom.[37] The first coordination configuration of Zn is the ZnO_4 tetrahedron in ZnO. The increase of the white line intensity implies the increase of coordination of oxygen around Zn, which could only result from the decreasing of V_O density.[38]

In Figure 7 we compared the variation of intensity of the peak at 643 cm^{-1} in Raman spectra (I_{R643}), the intensity of

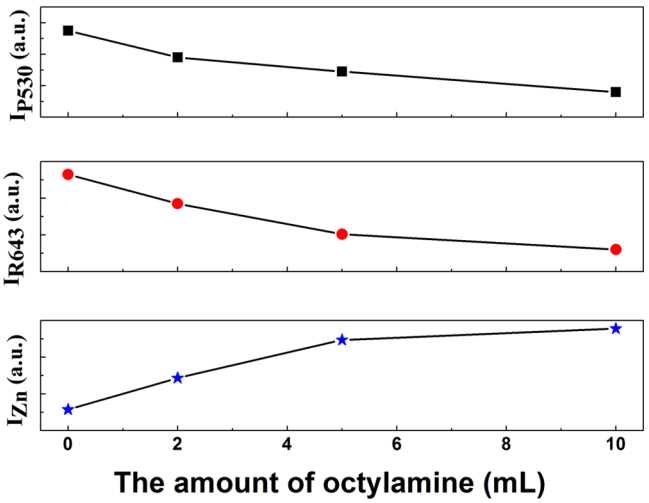

Figure 7. Variation of intensity of peak B in Raman spectra (I_{R643}), the intensity of green emission at about 530 nm in PL spectra (I_{P530}), and the intensity of the white line in Zn k-edge XANES spectra (I_{Zn}) of $Zn_{0.98}Mn_{0.02}O$ nanocrystalline treated with different octylamine.

green emission at about 530 nm in PL spectra (I_{P530}), and the intensity of the white line in Zn k-edge XANES spectra (I_{Zn}) of $Zn_{0.98}Mn_{0.02}O$ nanocrystals treated with different octylamine. As we discussed above, all these peaks are related with the V_O density. The decrease of I_{R643} and I_{P530} and the increase of I_{Zn} reveal that the V_O density deceases with increasing treatment of octylamine content. All these results are well consistent with each other.

Figure 8 shows the Mn k-edge Fourier transform of $k^3\chi(k)$ functions without phase correction for our samples. For comparison, the Mn k-edge Fourier transform of $k^3\chi(k)$ functions of Mn metal, MnO, Mn_2O_3, and MnOOH as well as the Zn k-edge of pure ZnO are also illustrated. Here, peaks A_1 (1.41 Å) and B_1 (2.41 Å) could be attributed to the first Mn−O and the second Mn−Mn coordination shell of MnO_6 in MnOOH, respectively, and the elongated $Mn^{3+}O_6$ octahedron[39] has two long and four short Mn−O bonds, as shown in Figure 9(a). Peaks A_2 (1.55 Å) and B_2 (2.87 Å) represent the first Zn−O and the second Zn−Zn shell in ZnO. With Mn substituting Zn, the coordination of Mn in Mn-doped ZnO is a $Mn^{2+}O_4$ tetrahedron with four identical Mn−O bonds, as shown in Figure 9(b). In untreated nanocrystals, there are only two peaks located at 1.41 and 2.41 Å, which means that there are only MnO_6 configurations. In octylamine-treated samples, there are three main coordination peaks, as shown in Figure 8. Peak A corresponds to the Mn−O coordination, which is situated between peaks A_1 and A_2. The other two peaks are located at around 2.41 and 2.87 Å, close to peaks B_1 and B_2,

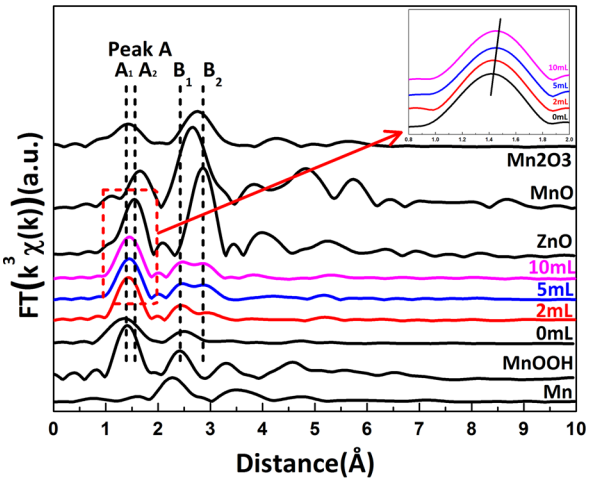

Figure 8. Mn k-edge Fourier transform of XAFS $k^3\chi(k)$ functions for $Zn_{0.98}Mn_{0.02}O$ nanocrystals treated with different content of octylamine and Mn, MnO, Mn_2O_3, and MnOOH reference samples, together with the Zn k-edge of reference ZnO. Inset is a comparison of peak A for the four samples.

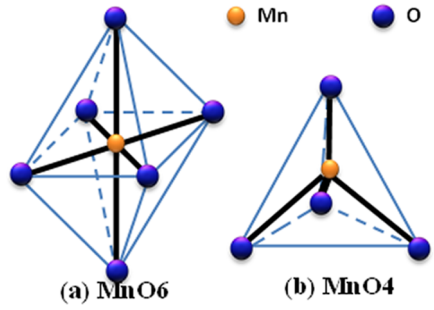

Figure 9. Schematic diagrams of MnO_6 (a) and MnO_4 in Mn-doped ZnO (b).

which represent the Mn−Mn in MnO_6 and the Mn−Zn(Mn) coordination in MnO_4 in $Zn_{0.98}Mn_{0.02}O$. The position of peak A situated between peak A_1 and A_2 as well as the coexistence of peaks at 2.41 and 2.87 Å indicate that there are two different configurations of Mn in octylamine-treated $Zn_{0.98}Mn_{0.02}O$ nanocrystals ($Mn^{2+}O_4$ and $Mn^{3+}O_6$ configurations, respectively). With increasing treatment of octylamine content from 2 to 10 mL, the position of peak A shifts from 1.43 to 1.49 Å, as shown in the inset. The increase of Mn−O bonding distance indicates that the content of Mn-substituted Zn in $Zn_{0.98}Mn_{0.02}O$ nanocrystals is increasing, while the concentration of MnO_6 is decreasing. In addition, the increasing intensity of the peak at 2.87 Å provides another evidence for the increase of MnO_4 in $Zn_{0.98}Mn_{0.02}O$ nanocrystals.

Figure 10 shows the normalized Mn k-edge XANES spectra of $Zn_{0.98}Mn_{0.02}O$ nanocrystals treated with different content of octylamine and the reference samples of Mn, MnO, and Mn_2O_3, respectively. For comparison, the Zn k-edge XANES spectrum of reference ZnO is shifted to the position of the Mn k-edge XANES spectra of $Zn_{0.98}Mn_{0.02}O$. The valence of Mn in Mn metal, MnO, and Mn_2O_3 varies from 0 to +3. The positions of the white line A in our samples are close to that of Mn_2O_3, which indicates that the valence of Mn is close to trivalent. However, with increasing octylamine treatment content from 2 to 10 mL, there is a small shift to the low energy white line A resulting from the increasing Mn^{2+} in $Zn_{0.98}Mn_{0.02}O$ nano-

dx.doi.org/10.1021/am301471v | ACS Appl. Mater. Interfaces 2012, 4, 4470−4475

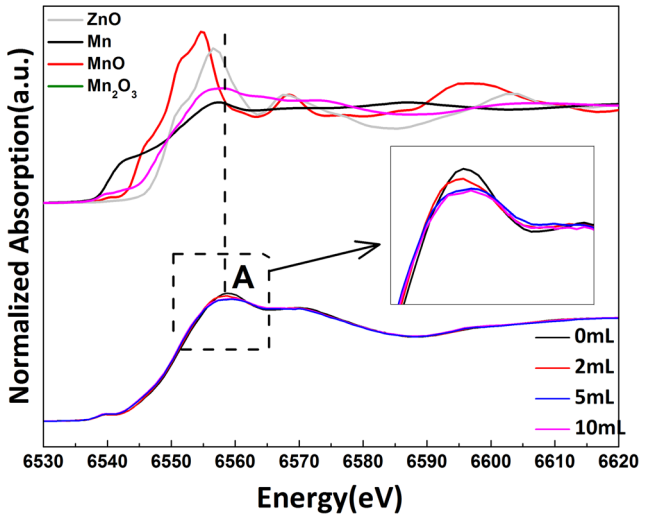

Figure 10. Normalized Mn k-edge XANES spectra of $Zn_{0.98}Mn_{0.02}O$ nanocrystals treated with different content of octylamine and reference samples Mn, MnO, and MnOOH. The Zn k-edge XANES spectrum of reference ZnO is shifted to the position of the Mn k-edge XANES spectra of the samples. The inset displays a comparison of the white lines of the four samples.

crystals, which is in agreement with the result of Mn k-edge EXAFS. In addition, the intensity of the white line for our samples decreases with increasing octylamine treatment content, which indicates that the number of O atoms around Mn decreases. So we conclude that the decrease in O content around Mn atoms in $Zn_{0.98}Mn_{0.02}O$ is due to the reduced coordination of Mn resulting from the transformation from MnO_6 to MnO_4.

Figure 11 shows the variation of intensity of the white line in Mn k-edge XANES spectra (I_{Mn}), the position of the white line in Mn k-edge XANES (P_W), the bond length of Mn−O, and the intensity of peak A in Raman spectra (I_{R521}) of $Zn_{0.98}Mn_{0.02}O$ nanocrystalline treated with different octylamine

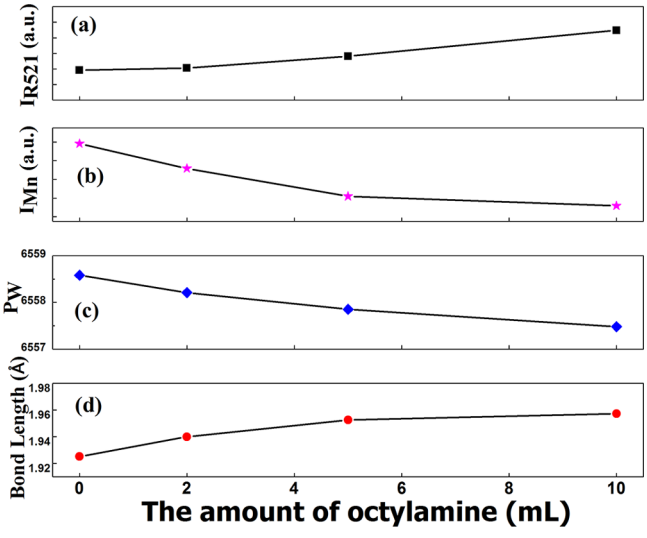

Figure 11. Variation of intensity of the white line in Mn k-edge XANES spectra (I_{Mn}), the position of the white line in Mn k-edge XANES (P_W), the bond length of Mn−O, and the intensity of peak A in Raman spectra (I_{R521}) of $Zn_{0.98}Mn_{0.02}O$ nanocrystalline treated with different octylamine content.

content. The bond lengths of Mn−O are deduced from Mn k-edge EXAFS spectra. The I_{R521} increases with increasing content of octylamine, as shown in Figure 11(a), indicating that the amount of MnO_4 increases and the concentration of MnO_6 decreases, which is further confirmed by the decrease of I_{Mn} and P_W as well as the increase of bond length of Mn−O, as shown in Figure 11 (b), (c), and (d).

From the above analysis, we can see that the Mn content in the lattice of ZnO increases with increasing octylamine content. There are two reasons to explain this phenomenon. First, codoping with N can enhance the solubility of Mn in ZnO. In the Mn-doped ZnO system, there is only a donor level in the band gap, and the estimated donor binding energy of impurity is high,[14] which induces the low Mn solubility in ZnO. The Bohr radius and binding energy of the donor are given by eqs 1 and 2, where ε is the dielectric constant; $\hbar$ is reduced Planck constant; and m_e and e are the effective mass and charge of the electron.

$$a_d = \frac{\varepsilon \hbar}{m_e e^2} \tag{1}$$

$$E_B = \frac{e^4 m_e}{2\varepsilon^2 \hbar^2} = \frac{e^2}{2\varepsilon} \cdot \frac{1}{a_d} \tag{2}$$

When codoping with N in $Zn_{0.98}Mn_{0.02}O$, an acceptor level will be formed. There will be hybridization between the acceptor and the donor. The donor impurity bandwidth will increase, and the effective mass of electron will decrease, which increases the Bohr radius of the Mn donor. According to eq 2, the binding energy of impurity will be lowered. As a result, the solubility of Mn in ZnO is enhanced by codoping N.[13−15] Second, the reducibility of octylamine may also decrease the amount of Mn^{3+} according to the reaction

$$Mn^{3+}O_6 \xrightarrow{\text{octylamine}} Mn^{2+}O_4 + 2O \tag{3}$$

When the $Zn_{0.98}Mn_{0.02}O$ nanocrystals are treated with more octylamine content, more Mn^{2+} would dissolve into ZnO. Meanwhile, more O would be released, and part of these O atoms may dissolve into the lattice and decreases V_O. In addition, N ions from octylamine occupy the sites of oxygen vacancies which will also decrease V_O.

4. CONCLUSION

We have synthesized N codoped $Zn_{0.98}Mn_{0.02}O$ nanocrystals by the wet chemical route and postoctylamine treatment. With increasing content of octylamine, N entering into ZnO lattice increases; the concentration of V_O decreases; and the content of Mn-substituted Zn in Mn-doped ZnO increases. The decrease of V_O is due to the oxygen vacancies that are occupied by the O atoms released from MnO_6 and the N ions from octylamine. The increasing solubility of Mn in ZnO is attributed to low donor binding energy resulting from the orbital hybridization between N-acceptor and Mn-donor level. We have clearly demonstrated that codoping with N can enhance the solubility of Mn in ZnO and suppress V_O density in $Zn_{0.98}Mn_{0.02}O$ nanocrystals. All results suggest that codoping is an effective method to enhance the solubility of transition metal and tune defects in oxide semiconductors.

■ ASSOCIATED CONTENT

Supporting Information

1. TEM image of the nanocrystals. 2. The comparison of lattice constant and Mn−O bond length of the samples treated with different content of octylamine. This material is available free of charge via the Internet at http://pubs.acs.org.

■ AUTHOR INFORMATION

Corresponding Author

*Tel. & Fax: +86-10-82339306. E-mail: whao@buaa.edu.cn (W. C. Hao). Tel. & Fax: +86-10-82317935. E-mail: hzxu@buaa.edu.cn (H. Z. Xu)

Notes

The authors declare no competing financial interest.

■ ACKNOWLEDGMENTS

The authors thank Dr. T. Silver for her useful discussions. This work was financially supported by the National Natural Science Foundation of China (Grant No. 51072012). The authors would like to thank Beamline 1W1B at the Beijing Synchrotron Radiation Facility for the measurements of Mn and Zn k-edge XAFS, as well as Prof. Jinghai Yang and Dr. Ming Gao for the Raman and PL measurements at Jilin Normal University. The authors would also thank Prof. Tao Liu for providing the Mn k-edge EXAFS data of reference MnOOH.

■ REFERENCES

(1) Üzgür, Ü.; Alivov, Y. I.; Liu, C.; Teke, A.; Reshchikov, M. A.; Doğan, S.; Avrutin, V.; Cho, S. J.; Morkoç, H. *J. Appl. Phys.* **2005**, *98*, 041301.

(2) Suchea, M.; Christoulakis, S.; Moschovis, K.; Katsarakis, N.; Kiriakidis, G. *Thin Solid Films* **2006**, *515*, 551−554.

(3) Dietl, T.; Ohno, H.; Matsukura, F.; Cibert, J.; Ferrand, D. *Science* **2000**, *287*, 1019−1022.

(4) Dalpian, G. M.; Chelikowsky, J. R. *Phys. Rev. Lett.* **2006**, *96*, 226802.

(5) Norris, D. J.; Efros, A.; Erwin, S. C. *Science* **2008**, *319*, 1776−1779.

(6) Zhang, J.; Skomski, R.; Sellmyer, D. J. *J. Appl. Phys.* **2005**, *97*, 10D303.

(7) Mahan, G. D. *J. Appl. Phys.* **1983**, *54*, 3825−3832.

(8) Sharma, V. K.; Varma, G. D. *J. Appl. Phys.* **2007**, *102*, 056105.

(9) Zhang, X. T.; Liu, X. C.; Zhang, J. Y.; Lu, Y. M.; Shen, D. Z.; Fan, X. W.; Kong, X. G. *J. Cryst. Growth* **2003**, *254*, 80−85.

(10) Park, S. H.; Minegishi, T.; Lee, H. J.; Park, J. S.; Im, I. H. *J. Appl. Phys.* **2010**, *108*, 093518.

(11) Chen, L. C.; Xiong, Z. H.; Wan, Q. X.; Li, D. M. *J. Phys.: Conf. Ser.* **2011**, *276*, 012158.

(12) Sato, K.; Bergqvist, L.; Kudrnovský, J.; Dederichs, P. H.; Eriksson, O.; Turek, I.; Sanyal, B.; Bouzerar, G.; Katayama-Yoshida, H.; Dinh, V. A; Fukushima, T.; Kizaki, H.; Zeller, R. *Rev. Mod. Phys.* **2010**, *82*, 1633−1690.

(13) Yamamoto, T.; Katayama-Yoshid, H. *Jpn. J. Appl. Phys.* **1997**, *36*, L80−L83.

(14) Yamamoto, T. *Thin Solid Films* **2002**, *420*−*421*, 100−106.

(15) Yamamoto, T.; Katayama-Yoshida, H. *Phys. B* **2001**, *302*−*303*, 155−162.

(16) Steven, D. C. *Los Alamos Sci.* **2000**, *26*, 422−435.

(17) Sun, Z. H.; Yan, W. S.; Zhang, G. B.; Oyanagi, H.; Wu, Z. Y.; Liu, Q. H.; Wu, W. Q.; Shi, T. F.; Pan, Z. Y.; Xu, P. S.; Xu, S.; Wei, S. Q. *Phys. Rev. B* **2008**, *77*, 245208.

(18) Hsu, H. S.; Huang, J. C. A.; Huang, Y. H.; Liao, Y. F.; Lin, M. Z.; Lee, C. H.; Lee, J. F.; Chen, S. F.; Lai, L. Y.; Liu, C. P. *Appl. Phys. Lett.* **2006**, *88*, 242507.

(19) Schwartz, D. A.; Norberg, N. S.; Nguyen, Q. P.; Parker, J. M.; Gamelin, D. R. *J. Am. Chem. Soc.* **2003**, *125*, 13205−13218.

(20) Bylsma, R. B.; Becker, W. M.; Kossut, J.; Debska, U.; Yoder-Short, D. *Phys. Rev. B* **1986**, *33*, 8207−8215.

(21) Iqbal, J.; Liu, X. F.; Majid, A.; Yu, R. H. *J. Supercond. Novel Magn.* **2011**, *24*, 699−704.

(22) Ji, G. H.; Gu, Z. B.; Lu, M. H.; Wu, D.; Zhang, S. T.; Zhu, Y. Y.; Zhu, S. N.; Chen, Y. F. *J. Phys.: Condens. Matter* **2008**, *20*, 425207.

(23) Dijken, A. V.; Meulenkamp, E. A.; Vanmaekelbergh, D.; Meijerink, A. *J. Lumin.* **2000**, *87*−*89*, 454−456.

(24) Iwata, K.; Fons, P.; Yamada, A.; Matsubara, K.; Niki, S. *J. Cryst. Growth* **2000**, *209*, 526−531.

(25) Gu, Z. B.; Lu, M. H.; Wang, J.; Wu, D.; Zhang, S. T.; Meng, X. K.; Zhu, Y. Y.; Zhu, S. N.; Chen, Y. F. *Appl. Phys. Lett.* **2006**, *88*, 082111.

(26) Wu, K. P.; Gu, S. L.; Tang, K.; Zhu, S. M.; Xu, M. X.; Zhang, R.; Zheng, Y. D. *J. Appl. Phys.* **2009**, *106*, 113710.

(27) Duan, L. B.; Zhao, X. R.; Liu, J. M.; Geng, W. C.; Xie, H. Y.; Chen, S. *J. Magn. Magn. Mater.* **2011**, *323*, 2374−2379.

(28) Cong, C. J.; Liao, L.; Liu, Q. Y.; Li, J. C.; Zhang, K. L. *Nanotechnology* **2006**, *17*, 1520−1526.

(29) Rajalakshmi, M.; Arora, A. K.; Bendre, B. S.; Mahamuni, S. *J. Appl. Phys.* **2000**, *87*, 2445−2448.

(30) Yang, L. W.; Wu, X. L.; Huang, G. S.; Qiu, T.; Yang, Y. M. *J. Appl. Phys.* **2005**, *97*, 014308.

(31) Zhong, H. M.; Wang, J. B.; Chen, X. S.; Li, Z. F.; Xu, W. L.; Lu, W. *J. Appl. Phys.* **2006**, *99*, 103905.

(32) Wang, J. B.; Zhong, H. M.; Li, Z. F.; Lu, W. *Appl. Phys. Lett.* **2006**, *88*, 101913.

(33) Bundesmann, C.; Ashkenov, N.; Schubert, M.; Spemann, D.; Butz, T.; Kaidashev, E. M.; Lorenz, M.; Grundmann, M. *Appl. Phys. Lett.* **2003**, *83*, 1974−1976.

(34) Alaria, J.; Bouloudenine, M.; Schmerber, G.; Colis, S.; Dinia, A.; Turek, P.; Bernard, M. *J. Appl. Phys.* **2006**, *99*, 08M118.

(35) Alaria, J.; Turek, P.; Bernard, M.; Bouloudenine, M.; Berbadj, A.; Brihi, N.; Schmerber, G.; Colis, S.; Dinia, A. *Chem. Phys. Lett.* **2005**, *415*, 337−341.

(36) Du, C. L.; Gu, Z. B.; You, Y. M.; Kasim, J.; Yu, T.; Shen, Z. X.; Ni, Z. H.; Ma, Y.; Cheng, G. X.; Chen, Y. F. *J. Appl. Phys.* **2008**, *103*, 023521.

(37) Lawniczak, J. K.; Iwanowski, R. J.; Golacki, Z.; Traverse, A.; Pizzini, S.; Fontanine, A.; Winter, I.; Hormes, J. *Phys. Rev. B* **1996**, *53*, 1119−1128.

(38) Zhang, S.; Zhang, L. J.; Li, H. M.; Li, J.; Jiang, Z.; Chu, W. S.; Huang, Y. Y.; Wang, J. Q.; Wu, Z. Y. *J. Synchrotron Radiat.* **2010**, *17*, 600−605.

(39) Kohler, T; Armbruster, T; Libowotzky, E. *J. Solid State Chem.* **1997**, *133*, 486−500.